Wang, Zulin; Hannula, Pyry-Mikko; De, Swarnalok; Wilson, Benjamin P.; Vapaavuori, Jaana; Yliniemi, Kirsi; Lundström, Mari

Controllable Production of Ag/Zn and Ag Particles from Hydrometallurgical Zinc Solutions

Published in:
ACS Sustainable Chemistry and Engineering

DOI:
10.1021/acssuschemeng.1c01789

Published: 21/06/2021

Document Version
Publisher's PDF, also known as Version of record

Please cite the original version:
Wang, Z., Hannula, P.-M., De, S., Wilson, B. P., Vapaavuori, J., Yliniemi, K., & Lundström, M. (2021). Controllable Production of Ag/Zn and Ag Particles from Hydrometallurgical Zinc Solutions. *ACS Sustainable Chemistry and Engineering*, *9*(24), 8186–8197. https://doi.org/10.1021/acssuschemeng.1c01789

ACS Sustainable Chemistry & Engineering
pubs.acs.org/journal/ascecg
Research Article

Controllable Production of Ag/Zn and Ag Particles from Hydrometallurgical Zinc Solutions

Zulin Wang, Pyry-Mikko Hannula, Swarnalok De, Benjamin P. Wilson, Jaana Vapaavuori, Kirsi Yliniemi, and Mari Lundström*

Cite This: *ACS Sustainable Chem. Eng.* 2021, 9, 8186–8197

Read Online

ACCESS | Metrics & More | Article Recommendations | Supporting Information

ABSTRACT: Ag/Zn and Ag particles have been successfully produced from electrolytes simulating zinc process solutions containing a high zinc concentration (65 g/L) and a negligible silver concentration (0.5–50 ppm) using a facile and sustainable electrodeposition-redox replacement (EDRR) method. Results show that the particle size and chemical composition of the deposited Ag/Zn and Ag particles can be readily controlled by varying the operating parameters such as replacement time and agitation. Electrochemical quartz crystal microbalance (EQCM) studies supported with SEM-EDS and TEM results indicate that the EDRR process consists of three regions: (I) zinc pulse deposition; (II) redox replacement between the Ag^+ ions and the deposited Zn, formation of a Zn/Ag alloy structure, and competing Zn oxidation by H^+ ions; and (III) further replacement between Ag^+ ions and Zn (alloy) formed in the previous stage and possible silver reduction by hydrogen. The Zn (alloy) has a higher reduction potential which hinders the competing H^+ reduction and sequentially improves the utilization efficiency of the sacrificial metal (Zn). Furthermore, by using the EDRR method, Ag/Zn particles could be successfully obtained from solutions with an extremely low Ag concentration of 0.5 ppm. The promising results demonstrate the feasibility of producing Ag-based functional materials utilizing trace amounts of Ag from zinc process solutions.

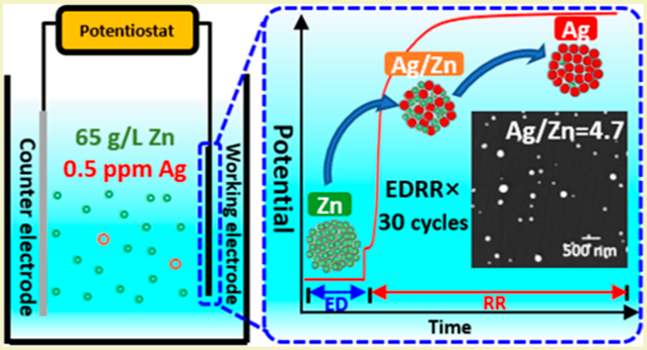

KEYWORDS: *Electrodeposition, Redox replacement, Precious metal, Circular economy, Bimetallic particles*

INTRODUCTION

Metallic nanoparticles are currently the subject of intensive research due to markedly different properties from their counterparts of bulk materials. In particular, the production of silver-based metallic nanoparticles has been an attractive field due to their superior conductive,[1] optical,[2] catalytic,[3] and especially antimicrobial properties.[4] The possibility of obtaining multifunctionality/enhanced properties by selecting the appropriate metal combinations has intrigued the investigation with broad bimetallic systems such as Ag/Pt,[5] Ag/Au,[6] Ag/Pd,[7] Ag/Cu,[8] Ag/Ni,[9] Ag/Zn,[10,11] and Ag/Fe[12] with the target of achieving new bifunctional or synergistic effects. For instance, Ag/Zn doped TiO_2 photocatalyst was found to have high efficiency toward ethyl phydroxybenzoate removal by photocatalysis (99.1% degradation within 2 h).[11] Moreover, Reyes-Vidal et al. reported the potential of Ag/Zn nanoparticles in antimicrobial applications that up to 98% of inhibition of bacterial growth was achieved after 30 min of contact time.[10] Various approaches have been proposed to prepare bimetallic nanoparticles including a galvanic replacement reaction,[5] electrodeposition and redox replacement,[13,14] colloidal synthesis,[6] calcination,[9] electrodeposition,[10] and coreduction of metal ions.[15] Among these methods, the electrodeposition and redox replacement (EDRR) method is of great interest because it offers the possibility to control the size and composition of bimetallic nanoparticles—which have significant impact on their properties and functionalities—in a facile manner. Moreover, EDRR does not involve the use of additional chemicals like reductants, thereby decreasing the potential environmental burden.

Redox replacement reactions have been investigated for decades to create noble metal (Ag, Au, Pt, Pd) mono/multilayers using a surface-limited redox replacement (SLRR) method that combines the underpotential deposition (UDP) of less noble metals (Zn, Cu, Ni, Pb).[16−19] Introduced first by Brankovic et al.,[20] the SLRR approach has been used to prepare functional materials with various applications in catalysts, sensors, fuel cells, and thin films.[21] Recent studies have also demonstrated the feasibility of the production of

Received: March 16, 2021
Revised: May 26, 2021
Published: June 8, 2021

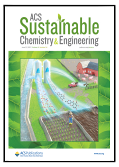

precious metal-based nanoparticles using the one-cell electrodeposition and redox replacement process.[13,14] However, these works are usually conducted under strictly controlled experimental conditions such as deoxygenation and optimized solution composition. On the other hand, the cost of nanoparticle production using traditional sources is expected to increase due to the ever-increasing demand of precious metals and depletion of high-grade raw materials. For instance, the consumption of silver has rapidly increased due to its demand in numerous applications like photographic, medical, electrical, electronics, chemical, jewelry, and especially recently solar cells.[22−26] In order to obtain silver sources for these industries, hydrometallurgical processes for silver separation by solvent extraction,[27] ion exchange,[28] and sorption[29] and for silver recovery by electrowinning,[30−32] chemical reduction,[33] precipitation,[34] and cementation[35−38] have all been studied for both primary and secondary raw materials. Nevertheless, application of these methods has become progressively difficult due to the related economic and environmental concerns, like depletion of high-grade raw materials and the increasingly complex feedstocks utilized in silver production. For instance, the specific energy consumption of electrowinning drastically increases with reduced silver concentration,[30,32] whereas other conventional processes usually involve the usage of additional chemicals that may increase the related wastewater outputs.

Based on green chemistry principles, we have introduced the electrodeposition and redox replacement (EDRR) method to the field of metal recovery—which has been proven successful in the recovery of minute concentrations of valuable elements (Ag, Au, Pt, and Te) from a variety of complex solutions.[39−45] Nonetheless, research is still in progress to develop a cost-effective and sustainable eco-efficient process for the valorization of secondary raw materials that contain only minor concentrations of precious metals. Our recent studies have demonstrated EDRR as a promising approach for the production of high value-added Ag/Cu nanoparticles from copper electrolytes and Pt/Ni cocatalysts from nickel process solutions.[46,47] The combination of Ag with the base metal Zn is of particular interest due to the currently underutilized low levels of silver (ppb to ppm level) that exist in large-scale industrial zinc process solutions.[48] Direct preparation of Ag/Zn nanoparticles from these solutions not only enhances the potential properties of the nanoparticles, but also improves the efficiency of silver utilization as a further step toward enhanced metal circulation within a global circular economy.

This study investigates the controllable preparation of Zn/Ag particles from hydrometallurgical zinc process solutions that contain minor concentrations of Ag (2−50 ppm) and a high concentration of Zn (65 g/L) using the electrodeposition and redox replacement (EDRR) method. The whole process was performed in a one-cell configuration without the need for the addition of extra chemicals. Deposited Zn/Ag particles were characterized using different analytical techniques such as scanning electron microscopy with energy dispersive X-ray spectroscopy (SEM-EDS) and transmission electron microscopy (TEM). The results show that the composition and size distribution of Zn/Ag particles can be determined by variation of operating parameters like the replacement time and agitation. Investigation with an electrochemical quartz-crystal microbalance (EQCM) revealed that the composition of Ag/Zn particles is affected not only by the redox replacement reaction between Ag ions and Zn but also by an intermediate Zn/Ag alloy formed during the replacement reaction and the competing dissolution of zinc by H^+ ions. Furthermore, the successful and controllable production of Ag/Zn particles from the solution that contain an extremely low concentration (0.5 ppm) of silver highlights the significant industrial application potential for the EDRR method.

EXPERIMENTAL SECTION

Solutions simulating industrial hydrometallurgical zinc solutions consisted of 65g/L Zn and 10 g/L H_2SO_4 while the Ag content was varied (0, 0.5, 2, 10, 50 ppm). Additionally, a blank solution containing 50 ppm Ag and 10 g/L H_2SO_4 was made to investigate the redox behavior of the Ag^+/Ag pair. All the solutions were prepared with Millipore Milli-Q deionized water (DI water, ≥18 MΩ·cm). Electrochemical experiments were carried out in a standard three-electrode cell (50 cm^3) at room temperature. Glassy carbon (GC) plates with a total surface area of 2 cm^2 (Alfa Aesar, U.S.A.) were utilized as the working electrode, and a platinum sheet (10 cm^2) was utilized as the counter electrode (≥99.5 wt % Pt, Kultakeskus Oy, Finland), while the reference electrode was a saturated mercury−mercurous sulfate electrode (Hg/Hg_2SO_4, +0.650 V vs a standard hydrogen electrode (SHE), Mettler Toledo, Switzerland). All the electrochemical measurements were controlled and monitored using an IviumStat 24-bit CompactStat potentiostat (Ivium Technologies, Netherlands). Prior to the electrochemical measurements, the GC electrodes were cleaned using ethanol under sonication for 20 min, rinsed with DI water, and cleaned in a 0.1 M H_2SO_4 solution by 10 cycles of cyclic voltammetry between −1000 mV and +1000 mV vs Hg/Hg_2SO_4, at a scan rate of 50 mV/s. After cleaning, the electrodes were thoroughly rinsed with DI water and dried in air.

In order to confirm the occurrence of the redox replacement, cementation experiments were carried out as a reference: zinc particles were first deposited on glassy carbon using pulse deposition from a zinc electrolyte in the absence of Ag^+ ions (65 g/L Zn and 10 g/L H_2SO_4), and the resulting surfaces—covered with Zn particles—were immersed in electrolytes that contained various concentrations of silver ions (65 g/L Zn, 10 g/L H_2SO_4, and 2−50 ppm Ag) for 200 s.

Ag and Ag/Zn particles were formed by 30 cycles (*n*) of repeated electrodeposition and redox replacement (EDRR) steps. A single EDRR event consisted of Zn particle electrodeposition (0.5 s potential pulse) followed by a galvanic replacement between Ag and Zn at the open circuit potential (OCP) for a desired replacement time of 0.5−200 s (*t*). The deposition potential values (*E*, between −1.55 and −1.60 V vs Hg/Hg_2SO_4) for zinc particle formation were selected based on cyclic voltammetry (CV) investigations undertaken in zinc solutions with similar Ag concentrations (0−50 ppm) that involved polarization sweeps initiated in the cathodic direction starting from 0 V (vs Hg/Hg_2SO_4) within a potential window of −1.700 V to +0.300 V (vs Hg/Hg_2SO_4) at a scan rate of 20 mV/s. Cyclic voltammetry measurements in the blank solution (50 ppm Ag and 10 g/L H_2SO_4) were conducted between −0.5 and +0.3 V (vs Hg/Hg_2SO_4) at a scan rate of 20 mV/s. In some experiments stirring was applied during the EDRR process with a magnetic stirring bar at 200 rpm. Additional experiments with different EDRR cycles or longer replacement times can be found in the Supporting Information.

Electrochemical quartz crystal microbalance (EQCM) measurements were undertaken using a Q-Sense E4 QCM System equipped with a QEM 401 electrochemistry module (Biolin Scientific, Sweden) in the 50 ppm Ag, 65g/L Zn, and 10 g/L H_2SO_4 solution (EDRR parameters: 0.5 pulse deposition at −1.55 V, 50 s replacement time, and 30 repetitive cycles). The working electrode was a 5 MHz gold coated AT-cut quartz crystal (surface area (A) = 1.13 cm^2). A platinum sheet (A = 3.08 cm^2) was used as the counter electrode, and a Ag/AgCl electrode (sat. KCl, +0.197 V vs SHE) as the reference. The mass (Δm) of the deposited Ag and Ag/Zn particles was determined using the Sauerbrey relation (eq 1), and the ratio M/z can be calculated via eq 2:

$$\Delta m = -(C_f \times \Delta f) \tag{1}$$

$$\frac{M}{z} = \frac{\Delta m \times F}{Q} \tag{2}$$

where C_f is a constant, C_f = 20 ng/Hz for an AT-cut 5 MHz quartz crystal with an active surface area of 1.13 cm^2, Δf is the frequency change, M is the molar mass of the deposit, F is Faraday's constant (96 485 C/mol), and Q is the electric charge during the pulse deposition.

From the perspective of silver recovery, the current efficiency (*CE*) of *n* EDRR cycles can be calculated using the following eq 3

$$CE = \frac{\Delta m\ (measured)}{\Delta m\ (theoretical)} \tag{3}$$

where Δm (measured) is the estimated mass change of Ag from the EQCM data (Zn is negligible according EDS results) and Δm (theoretical) is calculated from Faraday's law:

$$\Delta m\ (theoretical) = \frac{Q \times M_{Ag}}{z \times F} \tag{4}$$

where z is the valence of the atom reduced in the reaction (+1 for Ag^+ reduction). Consequentially, the current efficiency (*CE*) of *n* EDRR cycles can be estimated by eq 5, and the silver recovery efficiency (*RE*) can be calculated via eq 6:

$$CE = \frac{\Delta m_n \times F}{Q \times M_{Ag}} \tag{5}$$

$$RE = \frac{\Delta m_n}{V \times c} \tag{6}$$

where Δm_n is the mass change of Ag from n EDRR cycles, M_{Ag} is the molar mass of Ag (107.9 g/mol), V is the volume of the zinc process solutions, and c is the concentration of Ag (g/L).

The morphology and composition of the EDRR samples were characterized using scanning electron microscopy (SEM, Mira^3 Tescan GM, Czech Republic) equipped with energy-dispersive X-ray spectroscopy (EDS, ThermoFisher Scientific Ultradry EDS Detector, U.S.A.). The reported particle composition (Ag atom %) was an average value of the EDS results from at least 10 particles per sample. SEM micrographs with magnifications of 20 000 and 50 000 were selected for the particle size analysis using ImageJ software, and a minimum of 100 particles were analyzed per sample. The variations of the results are presented—where appropriate—as standard deviation. Transmission electron microscopy (TEM, JEOL JEM-2800) with large angle energy dispersive spectrometry (EDS) was also used to further examine the microstructure and element distribution of selected samples that were prepared by EDRR using carbon coated copper grids as the working electrode.

RESULTS AND DISCUSSION

Redox Replacement between Ag and Zn. The redox replacement reaction spontaneously occurs between Zn^0 and Ag^+ ions, and the driving force of the reaction under standard conditions is attributed to the potential difference of 1.5614 V between Zn^{2+}/Zn and Ag^+/Ag (eqs 7 and 8):

$$Zn^{2+}_{aq} + 2e^- \rightarrow Zn(s) \quad E^0 = -1.4118\ V \text{ vs } Hg/Hg_2SO_4 \tag{7}$$

$$Ag^+_{aq} + e^- \rightarrow Ag(s) \quad E^0 = +0.1496 \text{ V vs } Hg/Hg_2SO_4 \tag{8}$$

Nevertheless, the equilibrium potential of the redox pair will exhibit a shift from the standard values under actual experimental conditions. For instance, the deposition potential of Zn is usually more negative than the standard potential of the Zn^{2+}/Zn pair due to a nucleation overpotential.[49] In order to investigate the redox replacement reaction between Zn^0 and Ag^+ ions and identify the suitable deposition potential (*E*) required for the EDRR protocol, cyclic voltammograms (CV) of a GC electrode were measured in zinc electrolytes in the absence and presence of Ag^+ ions (2, 10, and 50 ppm) (Figure 1). Additional CVs were also carried out in the blank solution with a potential range of −0.5 V to +0.3 V (vs Hg/Hg_2SO_4) to investigate the redox behavior of the Ag^+/Ag pair.

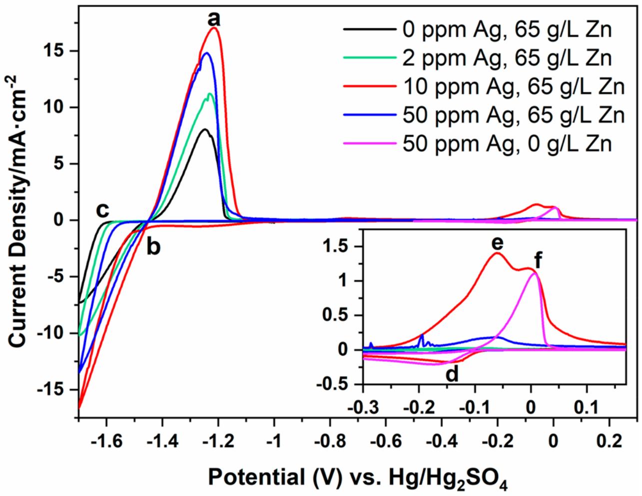

Figure 1. Cyclic voltammograms (scan rate: 20 mV/s) of a glassy carbon electrode in a blank solution (50 ppm Ag and 10 g/L H_2SO_4) and zinc electrolytes containing 65 g/L Zn, 10 g/L H_2SO_4, and various concentrations (0, 2, 10, and 50 ppm) of Ag^+ ions. Peak "a" is the zinc dissolution peak, point "b" is the crossover potential, point "c" is the nucleation potential, "d" is the Ag deposition peak, "e" is the stripping of the Zn/Ag alloy, and "f" is the stripping of Ag.

In the cathodic scan, zinc reduction starts to appear at point "c"—known as the nucleation potential—while the anodic peak at point "a" corresponds to the dissolution of zinc deposited during the reverse scan. The potential difference between the nucleation potential and crossover potential (point "b") is known as the nucleation overpotential (NOP), and high NOP values indicate strong polarization.[50,51] It can be seen from the CV curves that Ag^+ ions have marked depolarization effects on the cathode. For instance, the Zn nucleation potential is shifted toward the anodic direction from −1.62 V (vs Hg/Hg_2SO_4, NOP = 170 mV) in the absence of Ag^+ to −1.51 V (vs Hg/Hg_2SO_4, NOP = 60 mV) with the addition of 50 ppm of Ag. In the more positive potential range, a cathodic peak corresponding to Ag reduction was detected at −0.12 V (vs Hg/Hg_2SO_4) (d), even though it becomes less noticeable with lower Ag concentrations. Moreover, a clear difference was observed in the anodic scans between the zinc solution (65 g/L Zn and 50 ppm Ag) and the blank solution (50 ppm Ag only). The anodic peak (f) in both solutions is due to silver oxidation, while the second anodic peak (e) in the Zn solution (65 g/L Zn and 50 ppm Ag) is believed to be associated with the stripping of the Zn−Ag alloy. A similar phenomenon has also been found in a previous study with platinum substrates,[45] which indicates that the alloy structure formation is independent of the electrode material used.

Metallic zinc powders are commonly used as an electron donor for the recovery of silver from hydrometallurgical streams via traditional, nonpulsed redox replacement (i.e., cementation).[35−38,52] However, the redox replacement process between as-prepared zinc particles and Ag^+ ions has not been the subject of any intense investigation. Moreover, cementation processes in previously published studies are usually practiced with relatively high concentrations of silver (hundreds of ppm to g/L level).[35−38,52] In order to investigate the redox replacement reaction in solutions with only minor amounts of Ag (as low as 2 ppm), the following investigation was conducted: Zinc particles were first deposited on GC electrodes from a silver-free zinc electrolyte using 20 cycles of pulse deposition, where one cycle of pulse deposition consists of 0.5 s of potential pulse at −1.65 V, followed by an open circuit potential for 0.5 s. As shown in Figure 2A, zinc particles (Zn atom % > 99.5%) obtained via pulse deposition were found to have a hexagonal structure. A similar morphology has been commonly observed during zinc deposition, and this is possibly due to a lower thermodynamic free energy related to the exposed closest packed plane in hexagonal close-packed (hcp) metals.[53−56] The GC electrodes deposited with Zn particles were immersed sequentially in solutions containing 50, 10, and 2 ppm of silver for 200 s (i.e., cementation). The subsequent EDS results indicate that the samples were mostly silver particles with a spherical morphology as shown in Figure 2B−D. A decrease of particle sizes with lower silver concentration was observed, and similar phenomena have been reported previously for Ag/Cu particles.[47] This observation is possibly due to the competing reduction of H^+ shown in eq 9, as the potential of the Ag^+/Ag pair shifted to the negative direction according to Nernst equation, whereas the potential of H^+/H_2 remained unchanged.

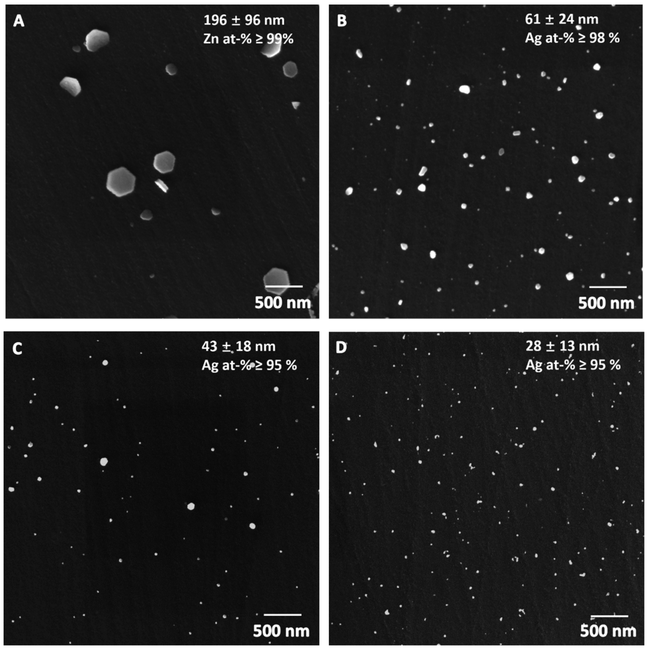

Figure 2. SEM micrographs of (A) Zn particles by 20 cycles of pulse deposition (−1.65 V followed by the open circuit potential for 0.5 s) from Zn electrolyte (65 g/L Zn, 10 g/L H_2SO_4) and samples by cementation from solutions containing 65 g/L Zn, 10 g/L H_2SO_4, and varying concentrations of Ag for 200 s: (B) 50 ppm, (C) 10 ppm, and (D) 2 ppm.

$$2H^+_{aq} + 2e^- \rightarrow H_2(g) \quad E^0 = -0.650 \text{ V vs Hg/Hg}_2\text{SO}_4 \tag{9}$$

Ultimately, these results confirmed the occurrence of the redox replacement reaction of zinc particles with solution that contained as low as 2 ppm Ag^+ ions. On the other hand, this cementation process is carried out with a two-step configuration: Zinc is deposited first in a cell before a separate immersion to obtain silver particles, which leads to a relatively laborious operating procedure.

EDRR with Varying Redox Replacement Times. A typical potential−time profile recorded during the EDRR measurements is displayed in Figure 3A. Potential transients of 6 EDRR cycles from a total of 30 EDRR cycles are presented here for the purpose of clarity. In each EDRR cycle, Zn is first deposited on the GC substrate using a short potential pulse (ED step); this is succeeded by a redox replacement step (RR step) when the external voltage is removed for a desired duration (replacement time), and the system is left at the open circuit potential (OCP). During the RR step, Ag^+ ions are spontaneously reduced to the metallic form (Ag^0) by the deposited Zn due to the potential difference between the redox pairs Ag^+/Ag and Zn^{2+}/Zn. Several EDRR cycles (n) were repeated to form more particles on the surface of the GC electrodes. Particles with different compositions (Ag and Zn content) and morphologies can be obtained by controlling the

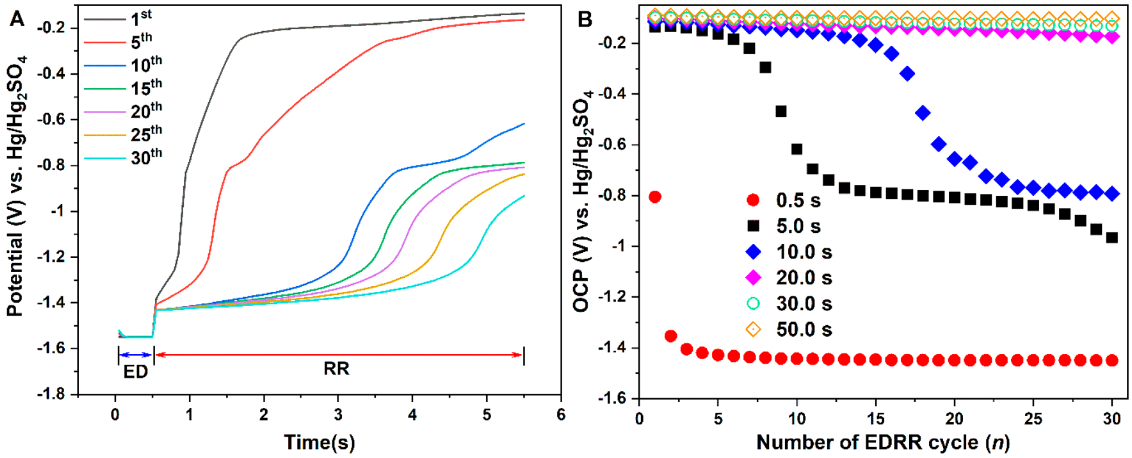

Figure 3. (A) Typical potential−time graph of the EDRR protocol in zinc solution with 50 ppm Ag (E = −1.55 V vs Hg/Hg_2SO_4, t_1 = 0.5 s, t_2 = 5 s, and n = 30). (B) Open circuit potential (OCP) values at the ends of the EDRR cycles with varying replacement times.

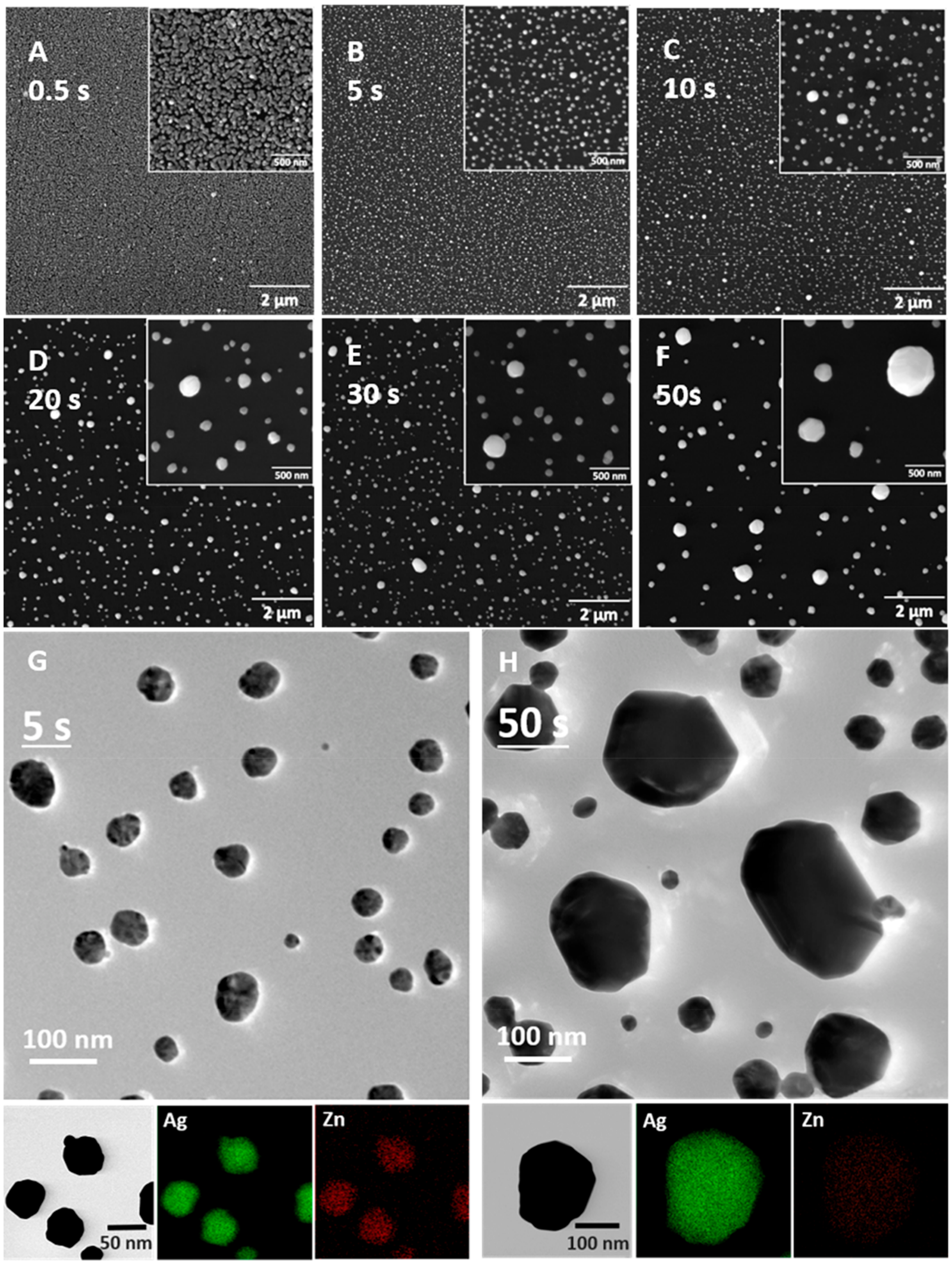

Figure 4. (A-F) SEM micrographs of GC electrodes after EDRR in solution containing 65 g/L Zn, 10 g/L H_2SO_4, and 50 ppm of Ag with varying replacement times ($E = -1.55$ V, $t_1 = 0.5$ s, $n = 30$ cycles); (G and H) TEM and EDS mapping images of EDRR samples with 5 and 50 s replacement times, respectively.

operating parameters such as the pulse potential (E), pulse deposition time (t_1), redox replacement time (t_2), and number of cycles (n).

Ag/Zn and Ag NPs were first prepared on GC electrodes using the EDRR method from zinc electrolytes (65 g/L Zn and 10 g/L H_2SO_4) containing 50 ppm Ag. The effect of the replacement time was investigated initially, and Figure 3B shows the compiled results of the OCP value at the end of each cycle from EDRR experiments with a replacement time of 0.5, 5, 10, 20, 30, and 50 s ($E = -1.55$ V vs Hg/Hg_2SO_4, $t_1 = 0.5$ s, and $n = 30$). The micrographs (SEM and TEM) of the particles produced by EDRR are shown in Figure 4, and the corresponding results of the particle size (average diameter) and chemical composition (Ag/(Ag + Zn) atom %, from the EDS results) are presented in Table 1 (N.B. particles from the 0.5 s replacement time are not clearly separated, and therefore the particle size was not analyzed).

As can been seen from Figure 4A, electrodeposition—with the minimal 0.5 s replacement time—results in almost pure Zn particles. A minor content of Ag was detected possibly because of a low level of replacement and/or the codeposition during the ED steps, and these results are in accordance OCP values as shown in Figure 3B. For the shortest RR time (0.5 s = red circles in Figure 3B), only the OCP of the first three cycles showed a mixed potential, i.e., the value between the potentials of pure Zn (ca. −1.45 V vs Hg/Hg_2SO_4) and pure Ag (ca. −0.09 V vs Hg/Hg_2SO_4) as observed from the CV measurements (Figure 1), while the rest have a similar OCP to pure Zn (ca. −1.45 V vs Hg/Hg_2SO_4). Furthermore, the related Zn particles also have a clearly different morphology

Table 1. SEM-EDS Quantitative Results of Particle Composition after EDRR Experiments with Varying Replacement Times (0.5−50 s) in Solution Containing 65 g/L Zn, 10 g/L H_2SO_4, and 50 ppm of Ag ($E = -1.55$ V, $t_1 = 0.5$ s, $n = 30$ cycles)

replacement time (s)	particle size (nm)	Ag (atom %)	Ag/Zn (atom ratio)
0.5	-	2.1 ± 0.8	<0.1
5	39 ± 16	67.1 ± 5.5	2.0
10	46 ± 22	87.8 ± 2.1	7.2
20	102 ± 40	89.8 ± 2.2	8.8
30	105 ± 48	94.9 ± 1.3	18.6
50	186 ± 100	96.9 ± 2.4	31.2

than those from the solution without silver (Figure 2A), and this could be attributed to the influence of Ag on the zinc nucleation process as also noted from the CV results in Figure 1. Clearly separated particles were obtained with longer replacement times (5−50 s) as shown in Figure 4B−F. This higher level of segregation between particles could result from some dissolution of the deposited material back into the solution due to the competing corrosion driven by H^+ ions. A comparable phenomenon has been observed in the formation of bimetallic Au/Cu nanorods using a galvanic replacement reaction.[57] As expected, the silver content in the particles increases as a function of the replacement time (Table 1). For instance, a material produced with a replacement time of 5 s contains 67.1 atom % of Ag, while a 50 s replacement time results in nearly pure Ag particles (96.9 atom %). The TEM images and high-resolution EDS mapping results are in good agreement with the SEM-EDS results and confirm that the silver content increases (as the Zn content decreases) with longer replacement times. Additionally, the OCP values of the working electrode showed a marked increase in the positive direction with extended replacement times, and this correlates with the higher silver content in the particles. A similar relationship between the particle composition and the OCP has also been found previously with Ag/Cu particles.[47] On the other hand, the reaction between Ag^+ and Zn shows much faster kinetics than that between the Ag^+ and Cu pair, which is probably due to the higher driving force (potential difference) between Ag^+ and Zn. Furthermore, unlike the core−shell structures with Ag/Cu nanoparticles by EDRR, the evenly distributed elements in individual particles (Figure 4G) suggests that the Ag/Zn particles formed with short replacement times have a mixed alloy structure.

An increase of particle size with replacement time was also noticeable, although the particles themselves have a less homogeneous distribution—highlighted by the higher standard deviation in Table 1. Conversely, a lower deviation of the particle distribution on the substrate surfaces was determined with a decreased replacement time, which can be associated with Ostwald ripening, and similar phenomenon has been observed in our previous studies about the preparation Ag/Cu particles and Pt/Ni particles.[46,47] Nevertheless, it is worth noting that the silver concentration in the solution is relatively low, and sequentially diffusion processes can have a marked influence on the reaction. For example, the diffusion of Ag^+ ions takes time, whereas H^+ ions are relatively abundant in the electrolytes and therefore the competing oxidation of Zn by H^+ during redox replacement cannot be ignored—hence, some particles might be oxidized by H^+ and dissolved back into the solution, which might also lead to a decrease in the electron transfer efficiency from Zn to the Ag^+ ions.

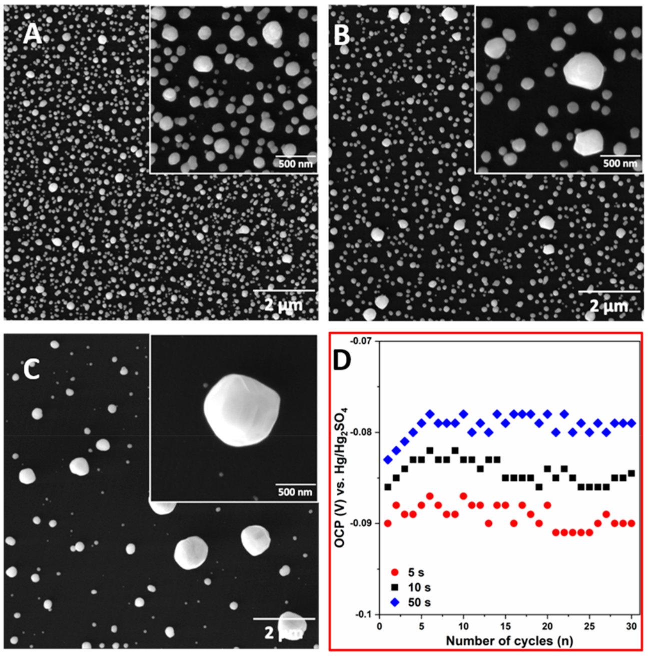

Figure 5. SEM of the working electrode after EDRR with 200 rpm of stirring ($E = -1.55$ V, $t_1 = 0.5$ s, $n = 30$ cycles, and replacement times of (A) 5 s, (B) 10 s, and (C) 50 s) and corresponding OCP values (D) in solution containing 65 g/L Zn, 10 g/L H_2SO_4, and 50 ppm of Ag.

Table 2. SEM-EDS Quantitative Results of the Particle Composition after EDRR Experiments with Varying Replacement Times with 200 rpm Stirring in Solution Containing 65 g/L Zn, 10 g/L H_2SO_4, and 50 ppm of Ag ($E = -1.55$ V, $t_1 = 0.5$ s, $n = 30$ cycles, and $t_2 = 5$, 10, and 50 s)

replacement time (s)	particle size (nm)	Ag (atom %)	Ag/Zn (atom)
5	114 ± 52	82.7 ± 3.9	4.8
10	134 ± 54	91.9 ± 3.7	11.4
50	252 ± 196	96.6 ± 1.2	28.4

Our earlier study with Ag/Cu nanoparticles found that stirring can significantly improve the mass transfer of the EDRR process and sequentially increase the product purity (Ag content) from the silver recovery point of view. Therefore, to investigate the effects of the diffusion process, further EDRR experiments were performed under agitation. Figure 5 shows the compiled EDRR results obtained with 200 rpm of stirring speed, and it is clear that the faster mass transfer improves the overall EDRR process as indicated by the rise in the silver concentration in the particles shown in Table 2 for samples with a short replacement time (5 and 10 s). For instance, the silver content of particles with a 5 s replacement time increased significantly from ca. 67 atom % (no agitation) to 82 atom % (200 rpm stirring). The recorded OCP values are also in agreement with the particle composition as the OCP of the working electrode with a short replacement time (5 and 10 s, Figure 5D) has significantly higher values compared to the results in the absence of stirring (Figure 3B). Without agitation, slightly more positive OCP values were recorded with a longer replacement time.

Nearly pure silver particles were obtained when the replacement time was further increased to 50 s, with OCP values slightly fluctuating at ca. −0.08 V vs Hg/Hg_2SO_4. Likewise, a further increase in the average particle size was also observed with agitation when compared to those obtained without stirring. One of the assumptions is that, with an enhanced mass transfer, a higher amount of zinc nuclei is deposited during the ED step, resulting in larger particles in the subsequent redox replacement step. On the other hand, when the stoichiometry of the redox replacement reaction—where two Ag^+ ions are required to replace one Zn^0—is considered, more Ag atoms are produced than previously deposited Zn atoms with a more complete reaction. Consequently, larger particle sizes are expected as shown previously with EDRR produced Ag/Cu nanoparticles.[47]

Process Mechanism. The previous section shows that Ag and Ag/Zn particles with various compositions and morphology can be prepared by the facile EDRR protocol through control of operating conditions like replacement time and agitation. Nevertheless, the underlying reaction mechanism responsible for these observations requires a more thorough investigation. Consequently, an additional investigation with the electrochemical quartz crystal microbalance technique (EQCM)—which can monitor the extremely sensitive mass variation during electrochemical processes—was utilized to further understand the mechanistic details during EDRR measurements.

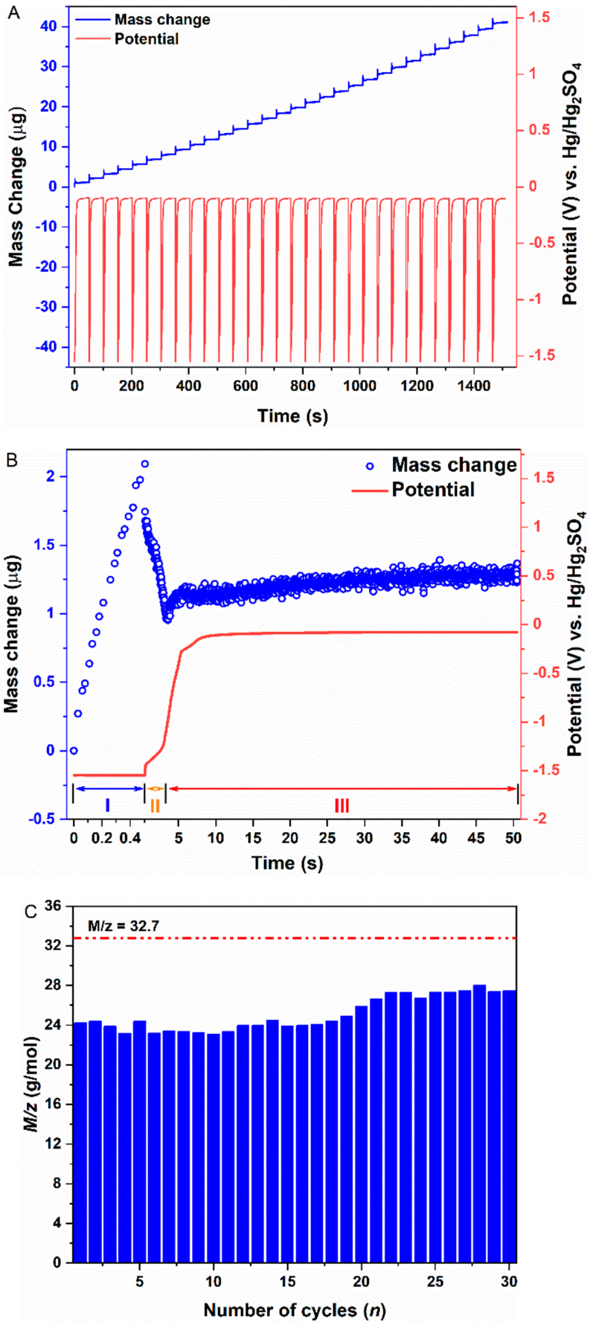

Figure 6. Mass change and potential transient during (A) 30 EDRR cycles; (B) one single EDRR cycle in solution containing 65 g/L Zn, 10 g/L H_2SO_4, and 50 ppm of Ag; and (C) M/z values during the electrodeposition steps ($E = -1.55$ V, $t_1 = 0.5$ s, $n = 30$ cycles, and $t_2 = 50$ s).

Figure 6 shows EQCM results that combine the potential and mass change as a function of time during EDRR measurements (0.5 s pulse deposition at −1.55 V with a replacement time of 50 s and 30 cycles of repetition). As can be seen in Figure 6A, the steady increase of the deposited mass during 30 cycles of EDRR experiments confirms the enrichment of Ag on the electrode. Three distinct regions can be identified in an enlarged single EDRR cycle (Figure 6B). Zinc deposition occurs in Region I (ED), indicated by a significant mass increase in the beginning 0.5 s. The molecular mass of the species involved in the ED step can be estimated by means of the mass/charge ratio (M/z). The side reactions can be characterized by the deviation between experimental M/z values and the expected theoretical value of hypothesized reaction. The experimental M/z values of the ED steps of 30 EDRR cycles are 23.9−28.1 g/mol (Figure 6C) and are lower than the theoretical value of zinc deposition (32.7 g/mol). This observation is commonly reported for zinc electrodeposition and is associated with the side reaction of H_2 evolution as well as electrical double layer formation, as the electric charge does not result in a mass increase in either process.[58]

The redox replacement of the zinc deposits to form Ag and Ag/Zn particles commences when the external potential is cut off. Considering that the zinc particles are replaced by heavier Ag atoms in a stoichiometric ratio of 1 to 2 (mass ratio Zn:Ag = 1:3.3), the deposit should have shown a steady positive mass increase assuming the electron transfer rate from Zn to Ag is 100% in the RR step. However, the RR step is split into two distinct regions according to the mass change: the mass shows a rapid decrease within a short time in Region II. The quantitative composition analysis of EDRR products with short replacement time (5 s) confirmed the occurrence of the replacement reaction between Zn and Ag^+, whereas the net mass decrease in Region II indicates a considerable amount of zinc is consumed by the competing H^+ reduction reaction (zinc stripping). The positive mass change in the following stage (Region III) further increases complexity of the mechanism details. In previous work with Au−Cu chloride solutions, the formation of copper(I) species after copper stripping can lead to a gradual mass increase in the latter stage of the RR step.[43] Nonetheless, when compared to the well-recognized copper(I) species—even if it has been found that the stripping of zinc consists of two consecutive steps ($Zn^0 \rightarrow Zn^+ \rightarrow Zn^{2+}$)[59]—the accumulation of a stable Zn (I) species in sulfate solution has yet to be reported. Therefore, the possibility of Ag^+ reduction by accumulated Zn (I) species in Region III is relatively unlikely, and the cyclic voltammetry results suggest that a Zn−Ag alloy structure is formed during the replacement reaction. Additionally, the Zn (alloy) has a higher redox potential than H_2/H^+, which hinders the oxidation (corrosion) of Zn (alloy) by H^+ ions and thus also hinders the relative speed of the mass decrease. Consequently, the net mass increase in Region III is believed to be primarily associated with the redox replacement between the Ag^+ and the Zn (alloy) on the surface. This is also supported by the further decrease of the Zn content (and increase of the Ag content) in Region III. Moreover, Ag reduction by hydrogen (H_2) in the solution phase can also occur proximal to the electrode surface, followed by the deposition on the surface as suggested by earlier surface limited redox replacement studies that used H_2 as an alternative reduction agent.[60] The mechanism of Ag particle formation using electrodeposition and redox replacement based on the EQCM study is presented schematically in Figure 7.

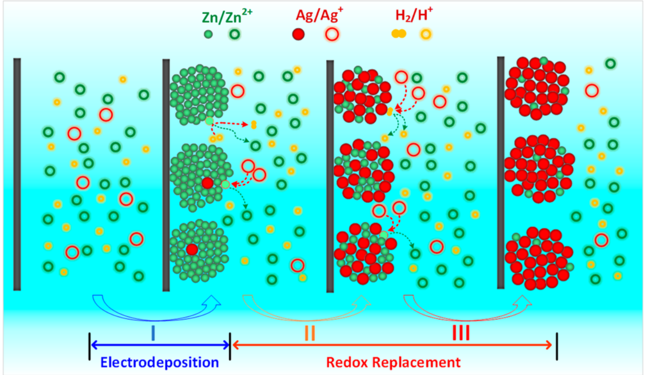

Figure 7. Schematic for the mechanism of Ag/Zn particle formation using electrodeposition and redox replacement (EDRR). Zn particles are deposited in region (I) (ED), followed by a redox replacement step (RR) at an open circuit potential comprising of regions (II) and (III): In region (II), redox replacement between Ag^+ and Zn^0 takes place simultaneously with the competing H^+ reduction to form a Ag/Zn alloy structure. Zn (alloy) is further replaced by Ag^+ in region (III), Ag^+ may also be reduced by H_2, and particles with high Ag content can be obtained.

The molar ratio between sacrificial metals and the noble metals is one of the most important parameters for the process evaluation of traditional cementation. For the EDRR process, the molar ratio of Zn deposited in the ED step and Ag obtained from each EDRR cycle is 2.3−2.6 (Zn:Ag), which is lower than most of the previously reported values for cementation.[35,36,38] In traditional cementation, the solution pH value is normally strictly controlled (≥3), and the noble metal concentration typically varies from hundreds of ppm to the g/L level; in contrast, the acid concentration during the EDRR process in this study is significantly higher and the silver concentration is only at a ppm level. These results suggest that although the purpose of this study is to prepare high value-added functional particles, the EDRR process also shows many significant advantages and a degree of flexibility for silver recovery when compared to regular cementation. From the perspective of silver recovery, the current efficiency (CE) over 30 EDRR cycles was 16.3%, and the silver recovery efficiency (RE) was 1.6% taking a 50 mL zinc solution with 50 ppm Ag as an example. It is worth noting that both current efficiency and recovery efficiency can be significantly improved when EDRR parameters are optimized specifically for silver recovery.[45]

Ag/Zn Particle Formation with a Minor Concentration of Ag. The industrial feasibility of the EDRR process was further investigated using zinc electrolytes with a lower silver concentration (10 ppm, 2 ppm, and extremely low to 0.5 ppm). As discussed in the previous section, agitation has significant impacts on the EDRR process with 50 ppm silver. Therefore, to improve the mass transfer condition, all the experiments with these lower silver concentrations were conducted with 200 rpm stirring. The compiled results of SEM images and OCP values are shown in Figure 8, while the particle composition and sizes are outlined in Table 3. As can be seen, Ag and Ag/Zn particles were successfully prepared using the EDRR method from solutions containing either a 10, 2, or 0.5 ppm Ag concentration. Like the results with 50 ppm Ag, the increase of the silver content and particle size with the greater diameter deviation was observed with longer replacement times. The OCP values also shift to the positive direction with longer replacement times for all the solutions with 0.5 to 10 ppm Ag, which is in accordance with the composition analysis gained from EDS. On the other hand, the reaction rate of redox replacement clearly shows a decreasing trend with a lower silver concentration. For instance, a 5 s replacement time is sufficient to obtain particles with a high Ag content (≥90 atom %) from a 50 ppm Ag solution, whereas the minimum replacement time required to achieve a similar silver percentage increases to 30 and 200 s for solutions with 10 and 2 ppm Ag, respectively. These slower reaction rates with much lower Ag concentrations can be attributed to the relative limitations of diffusion. In contrast, the potential of the Ag^+/Ag pair shifts to a negative direction with lower Ag concentration according to the Nernst equation, which decreases the driving force (potential difference of Ag^+/Ag and Zn^{2+}/Zn pairs) of the replacement reaction between Zn and Ag^+, which may have an impact on the reaction rate. It is worth noting that the content of silver can be further increased with a longer replacement time (Figure S2). Overall, these results demonstrate the feasibility of Ag and Ag/Zn particle formation using the EDRR method from hydrometallurgical-type solutions with dilute silver concentrations as low as 0.5 ppm.

■ CONCLUSIONS

This study presents a comprehensive investigation of Ag/Zn particle formation using repetitive EDRR cycles from simulated zinc process solutions with 65 g/L Zn, 10 g/L H_2SO_4, and 0.5−50 ppm Ag. A single EDRR cycle consists of two consecutive steps: (i) The sacrificial metal Zn is deposited by a 0.5 s potential pulse at a potential *E* which is determined from cyclic voltammetry studies. (ii) The external potential control is then disconnected for a time duration (i.e., replacement time), and the redox replacement between the more noble Ag^+ ions and the Zn particles spontaneously takes place due the potential difference of Ag^+/Ag and Zn^{2+}/Zn pairs. The effects of operating parameters including deposition voltage, replacement time, and stirring on the chemical composition and morphology of Ag/Zn particles were investigated through comprehensive experiments and analysis such as SEM-EDS, TEM, and OCP values.

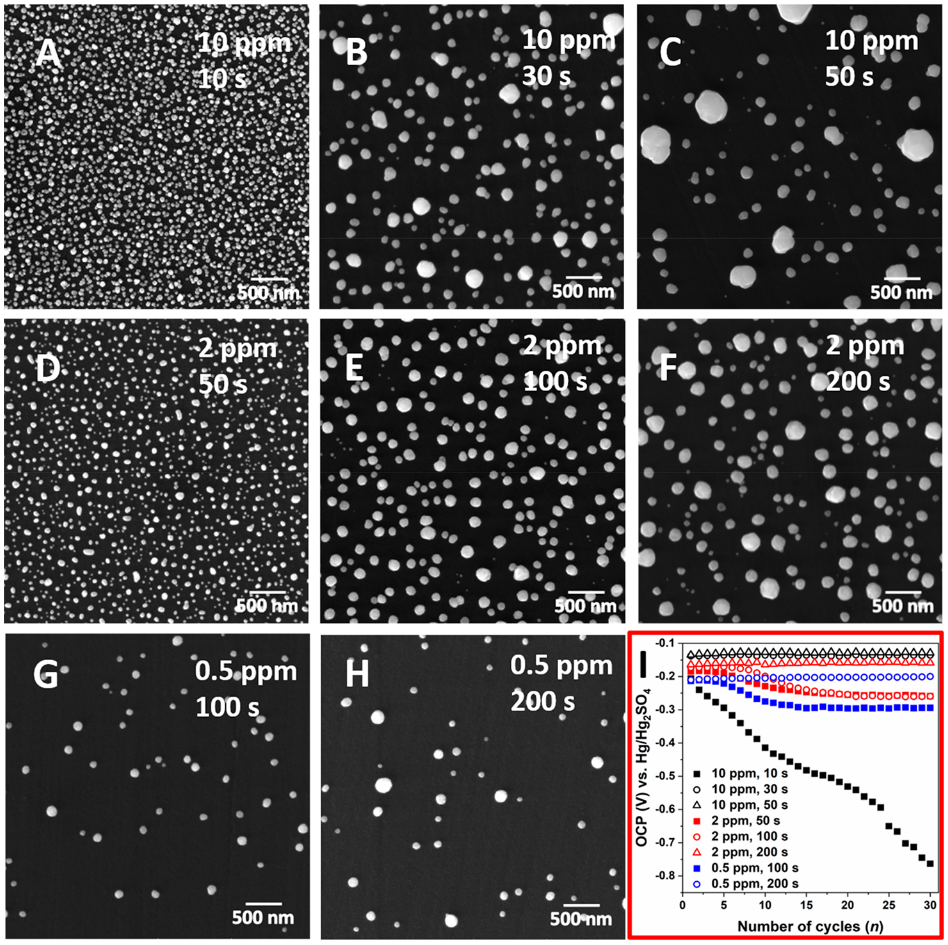

Figure 8. SEM micrographs of GC electrodes after EDRR experiments with a solution stirred at 200 rpm containing 65 g/L Zn, 10 g/L H_2SO_4, and (A−C) 10 ppm Ag, (D−F) 2 ppm Ag, and (G and H) 0.5 ppm Ag and (I) the corresponding OCP value of each EDRR cycle ($E = -1.60$ V, $t_1 = 0.5$ s, and $n = 30$ cycles).

Table 3. SEM-EDS Quantitative Results of the Particle Composition after EDRR Experiments with Varying Replacement Times: 200 rpm Stirred Solution Containing 65 g/L Zn, 10 g/L H_2SO_4 and 0.5−10 ppm of Ag ($E = -1.60$ V, $t_1 = 0.5$ s, and $n = 30$ cycles)

Ag concentration in solution	replacement time (s)	particle size (nm)	Ag (atom %)	Ag/Zn (atom ratio)
10 ppm	10	55 ± 20	48.7 ± 2.6	0.9
	30	131 ± 36	87.1 ± 3.1	6.8
	50	147 ± 87	92.3 ± 2.5	12.0
2 ppm	50	37 ± 22	49.1 ± 4.6	1.0
	100	126 ± 33	57.3 ± 3.3	1.3
	200	138 ± 63	85.7 ± 2.4	6.0
0.5 ppm	100	93 ± 25	54.2 ± 4.9	1.2
	200	109 ± 34	82.5 ± 3.2	4.7

By controlling the replacement time, the deposited zinc particles can be tuned to create bimetallic Ag/Zn particles with a mixed alloy structure and ultimately almost pure Ag particles. Longer replacement times also result in a larger particle size and more positive OCP values, while agitation can improve the mass transfer process and therefore increase the EDRR process kinetics. Further investigation of the process mechanism with EQCM revealed that three distinct regions (I)−(III) were present during a single EDRR cycle: the mass increase in region (I) confirmed the zinc deposition during the short potential pulse; the rapid mass decrease in region (II) indicates that redox replacement between Zn and Ag^+ ion took place simultaneously with competing reduction of H^+ ions (resulting in zinc stripping); and a gradual mass increase was recorded in region (III), which is believed to be associated with the redox replacement between Ag^+ and Zn (alloy) formed in the previous stage. Moreover, the possible Ag reduction by hydrogen (H_2) may also increase the mass change in region (III).

Overall, the successful and more sustainable production of Ag/Zn particles from solutions with extremely low Ag concentration (0.5 ppm) highlight the potential industrial feasibility of the EDRR process. Furthermore, these results demonstrate that the EDRR process is a promising technology for the valorization of trace amounts of valuable metals from base metal dominated process solutions and offers a facile route to the furtherance of the circular economy of metals.

■ ASSOCIATED CONTENT

Supporting Information

The Supporting Information is available free of charge at https://pubs.acs.org/doi/10.1021/acssuschemeng.1c01789.

Growth of Ag/Zn particles with different EDRR cycles and improved silver content in Ag/Zn particles with increased replacement time (PDF)

AUTHOR INFORMATION

Corresponding Author

Mari Lundström − *Department of Chemical and Metallurgical Engineering, School of Chemical Engineering, Aalto University, 02150 Espoo, Finland*; Email: mari.lundstrom@aalto.fi

Authors

Zulin Wang − *Department of Chemical and Metallurgical Engineering, School of Chemical Engineering, Aalto University, 02150 Espoo, Finland*; orcid.org/0000-0002-2234-7983

Pyry-Mikko Hannula − *Department of Chemical and Metallurgical Engineering, School of Chemical Engineering, Aalto University, 02150 Espoo, Finland*; orcid.org/0000-0001-9844-2234

Swarnalok De − *Department of Chemistry and Materials Science, School of Chemical Engineering, Aalto University, 02150 Espoo, Finland*

Benjamin P. Wilson − *Department of Chemical and Metallurgical Engineering, School of Chemical Engineering, Aalto University, 02150 Espoo, Finland*; orcid.org/0000-0002-2874-6475

Jaana Vapaavuori − *Department of Chemistry and Materials Science, School of Chemical Engineering, Aalto University, 02150 Espoo, Finland*; orcid.org/0000-0002-5923-0789

Kirsi Yliniemi − *Department of Chemistry and Materials Science, School of Chemical Engineering, Aalto University, 02150 Espoo, Finland*; orcid.org/0000-0003-2536-388X

Complete contact information is available at: https://pubs.acs.org/10.1021/acssuschemeng.1c01789

Notes

The authors declare no competing financial interest.

ACKNOWLEDGMENTS

Academy of Finland projects (GoldTail (319691) and NoWASTE (297962)) are greatly acknowledged for funding this research. The RawMatTERS Finland Infrastructure (RAMI) funded by the Academy of Finland and based at Aalto University is also acknowledged. In addition, the financial support from the Chinese Scholarship Council (CSC) is gratefully acknowledged by Z.W. S.D. was supported by the Ella and Georg Ehrnrooth Foundation. J.V. acknowledges with gratitude the funding from the Academy of Finland (SUPER-WEAR: Decision number: 322214 and SUBSTAINABLE: Decision number: 334818).

REFERENCES

(1) Li, Y.; Wu, Y.; Ong, B. S. Facile Synthesis of Silver Nanoparticles Useful for Fabrication of High-Conductivity Elements for Printed Electronics. *J. Am. Chem. Soc.* **2005**, *127* (10), 3266−3267.

(2) Evanoff, D. D.; Chumanov, G. Synthesis and Optical Properties of Silver Nanoparticles and Arrays. *ChemPhysChem* **2005**, *6* (7), 1221−1231.

(3) Xu, R.; Wang, D.; Zhang, J.; Li, Y. Shape-Dependent Catalytic Activity of Silver Nanoparticles for the Oxidation of Styrene. *Chem. - Asian J.* **2006**, *1* (6), 888−893.

(4) Xiu, Z.; Zhang, Q.; Puppala, H. L.; Colvin, V. L.; Alvarez, P. J. J. Negligible Particle-Specific Antibacterial Activity of Silver Nanoparticles. *Nano Lett.* **2012**, *12* (8), 4271−4275.

(5) Huang, Y.; Miao, Y.-E.; Ji, S.; Tjiu, W. W.; Liu, T. Electrospun Carbon Nanofibers Decorated with Ag−Pt Bimetallic Nanoparticles for Selective Detection of Dopamine. *ACS Appl. Mater. Interfaces* **2014**, *6* (15), 12449−12456.

(6) Sahu, S.; Sharma, S.; Ghosh, K. K. Novel Formation of Au/Ag Bimetallic Nanoparticles from a Mixture of Monometallic Nanoparticles and Their Application for the Rapid Detection of Lead in Onion Samples. *New J. Chem.* **2020**, *44* (35), 15010−15017.

(7) Jing, H.; Wang, H. Structural Evolution of Ag−Pd Bimetallic Nanoparticles through Controlled Galvanic Replacement: Effects of Mild Reducing Agents. *Chem. Mater.* **2015**, *27* (6), 2172−2180.

(8) Shin, K.; Kim, D. H.; Lee, H. M. Catalytic Characteristics of AgCu Bimetallic Nanoparticles in the Oxygen Reduction Reaction. *ChemSusChem* **2013**, *6* (6), 1044−1049.

(9) Pei, G. X.; Liu, X. Y.; Wang, A.; Su, Y.; Li, L.; Zhang, T. Selective Hydrogenation of Acetylene in an Ethylene-Rich Stream over Silica Supported Ag-Ni Bimetallic Catalysts. *Appl. Catal., A* **2017**, *545*, 90−96.

(10) Reyes-Vidal, Y.; Suarez-Rojas, R.; Ruiz, C.; Torres, J.; Ţălu, Ş.; Méndez, A.; Trejo, G. Electrodeposition, Characterization, and Antibacterial Activity of Zinc/Silver Particle Composite Coatings. *Appl. Surf. Sci.* **2015**, *342*, 34−41.

(11) Zhu, L.; Liu, X.; Wang, X.; Meng, X. Evaluation of Photocatalytic Selectivity of Ag/Zn Modified Molecularly Imprinted TiO2 by Multiwavelength Measurement. *Sci. Total Environ.* **2020**, *703*, 134732.

(12) Luo, S.; Yang, S.; Wang, X.; Sun, C. Reductive Degradation of Tetrabromobisphenol A over Iron−Silver Bimetallic Nanoparticles under Ultrasound Radiation. *Chemosphere* **2010**, *79* (6), 672−678.

(13) Zhang, G.; Kuang, Y.; Liu, J.; Cui, Y.; Chen, J.; Zhou, H. Fabrication of Ag/Au Bimetallic Nanoparticles by UPD-Redox Replacement: Application in the Electrochemical Reduction of Benzyl Chloride. *Electrochem. Commun.* **2010**, *12* (9), 1233−1236.

(14) Yliniemi, K.; Wragg, D.; Wilson, B. P.; McMurray, H. N.; Worsley, D. A.; Schmuki, P.; Kontturi, K. Formation of Pt/Pb Nanoparticles by Electrodeposition and Redox Replacement Cycles on Fluorine Doped Tin Oxide Glass. *Electrochim. Acta* **2013**, *88*, 278−286.

(15) Wu, M.-L.; Chen, D.-H.; Huang, T.-C. Preparation of Au/Pt Bimetallic Nanoparticles in Water-in-Oil Microemulsions. *Chem. Mater.* **2001**, *13* (2), 599−606.

(16) Venkatraman, K.; Gusley, R.; Yu, L.; Dordi, Y.; Akolkar, R. Electrochemical Atomic Layer Deposition of Copper: A Lead-Free Process Mediated by Surface-Limited Redox Replacement of Underpotentially Deposited Zinc. *J. Electrochem. Soc.* **2016**, *163* (12), D3008.

(17) Fayette, M.; Liu, Y.; Bertrand, D.; Nutariya, J.; Vasiljevic, N.; Dimitrov, N. From Au to Pt via Surface Limited Redox Replacement of Pb UPD in One-Cell Configuration. *Langmuir* **2011**, *27* (9), 5650−5658.

(18) Rettew, R. E.; Guthrie, J. W.; Alamgir, F. M. Layer-by-Layer Pt Growth on Polycrystalline Au: Surface-Limited Redox Replacement of Overpotentially Deposited Ni Monolayers. *J. Electrochem. Soc.* **2009**, *156* (11), D513.

(19) Mrozek, M. F.; Xie, Y.; Weaver, M. J. Surface-Enhanced Raman Scattering on Uniform Platinum-Group Overlayers: Preparation by Redox Replacement of Underpotential-Deposited Metals on Gold. *Anal. Chem.* **2001**, *73* (24), 5953−5960.

(20) Brankovic, S. R.; Wang, J. X.; Adžić, R. R. Metal Monolayer Deposition by Replacement of Metal Adlayers on Electrode Surfaces. *Surf. Sci.* **2001**, *474* (1), L173−L179.

(21) Dimitrov, N. Recent Advances in the Growth of Metals, Alloys, and Multilayers by Surface Limited Redox Replacement (SLRR) Based Approaches. *Electrochim. Acta* **2016**, *209*, 599−622.

(22) Syed, S. Silver Recovery Aqueous Techniques from Diverse Sources: Hydrometallurgy in Recycling. *Waste Manage.* **2016**, *50*, 234−256.

(23) Birloaga, I.; Vegliò, F. Overview on Hydrometallurgical Procedures for Silver Recovery from Various Wastes. *J. Environ. Chem. Eng.* **2018**, *6* (2), 2932−2938.

(24) Søndergaard, R. R.; Zimmermann, Y.-S.; Espinosa, N.; Lenz, M.; Krebs, F. Incineration of Organic Solar Cells: Efficient End of Life Management by Quantitative Silver Recovery. *Energy Environ. Sci.* **2016**, *9* (3), 857−861.

(25) Cho, S.-Y.; Kim, T.-Y.; Sun, P.-P. Recovery of Silver from Leachate of Silicon Solar Cells by Solvent Extraction with TOPO. *Sep. Purif. Technol.* **2019**, *215*, 516−520.

(26) Kuczyńska-Łażewska, A.; Klugmann-Radziemska, E.; Sobczak, Z.; Klimczuk, T. Recovery of Silver Metallization from Damaged Silicon Cells. *Sol. Energy Mater. Sol. Cells* **2018**, *176*, 190−195.

(27) Stankovic, V.; Outarra, L.; Zonnevijlle, F.; Comninellis, Ch Solvent Extraction of Silver from Nitric Acid Solutions by Calix[4]-Arene Amide Derivatives. *Sep. Purif. Technol.* **2008**, *61* (3), 366−374.

(28) Pavlinić, S.; Piljac, I. Electrolytic Desorption of Silver from Ion-Exchange Resins. *Water Res.* **1998**, *32* (10), 2913−2920.

(29) Elwakeel, K. Z.; Al-Bogami, A. S.; Guibal, E. 2-Mercaptobenzimidazole Derivative of Chitosan for Silver Sorption − Contribution of Magnetite Incorporation and Sonication Effects on Enhanced Metal Recovery. *Chem. Eng. J.* **2021**, *403*, 126265.

(30) Su, Y.; Li, Q.; Wang, Y.; Wang, H.; Huang, J.; Yang, X. Electrochemical Reclamation of Silver from Silver-Plating Wastewater Using Static Cylinder Electrodes and a Pulsed Electric Field. *J. Hazard. Mater.* **2009**, *170* (2), 1164−1172.

(31) Wang, Z.; Peng, C.; Yliniemi, K.; Lundström, M. Recovery of High-Purity Silver from Spent Silver Oxide Batteries by Sulfuric Acid Leaching and Electrowinning. *ACS Sustainable Chem. Eng.* **2020**, *8* (41), 15573−15583.

(32) Robinson, D.; Walsh, F. C. Silver Removal from an X-Ray Fixer Solution by Means of a Potentiostatically-Controlled Rotating Cylinder Electrode. *J. Photogr. Sci.* **1994**, *42* (6), 182−192.

(33) Chen, J. P.; Lim, L. L. Key Factors in Chemical Reduction by Hydrazine for Recovery of Precious Metals. *Chemosphere* **2002**, *49* (4), 363−370.

(34) Yazici, E. Y.; Yilmaz, E.; Ahlatci, F.; Celep, O.; Deveci, H. Recovery of Silver from Cyanide Leach Solutions by Precipitation Using Trimercapto-s-Triazine (TMT). *Hydrometallurgy* **2017**, *174*, 175−183.

(35) Viramontes Gamboa, G.; Medina Noyola, M.; López Valdivieso, A. Fundamental Considerations on the Mechanisms of Silver Cementation onto Zinc Particles in the Merril−Crowe Process. *J. Colloid Interface Sci.* **2005**, *282* (2), 408−414.

(36) Labra, M. P.; Pérez, M. R.; Serrano, J. A. R.; Dávila, E. O. Á.; Hernández, F. R. B.; Thangarasu, P. Silver Cementation with Zinc From Residual X Ray Fixer, Experimental and Thermochemical Study. In *Characterization of Minerals, Metals, and Materials 2016*; Ikhmayies, S. J., Li, B., Carpenter, J. S., Hwang, J.-Y., Monteiro, S. N., Li, J., Firrao, D., Zhang, M., Peng, Z., Escobedo-Diaz, J. P., Bai, C., Eds.; Springer International Publishing: Cham, 2016; pp 605−613, DOI: 10.1007/978-3-319-48210-1_76.

(37) Fabián, M.; Baláž, P.; Briančin, J. Study of the Silver Ions Cementation after Mechanical Activation of Cementator. *Hydrometallurgy* **2009**, *97* (1), 15−20.

(38) Liu, F.; Wang, J.; Peng, C.; Liu, Z.; Wilson, B. P.; Lundström, M. Recovery and Separation of Silver and Mercury from Hazardous Zinc Refinery Residues Produced by Zinc Oxygen Pressure Leaching. *Hydrometallurgy* **2019**, *185*, 38−45.

(39) Yliniemi, K.; Wang, Z.; Korolev, I.; Hannula, P.; Halli, P.; Lundström, M. Effect of Impurities in Precious Metal Recovery by Electrodeposition-Redox Replacement Method from Industrial Side-Streams and Process Streams. *ECS Trans.* **2018**, *85* (4), 59.

(40) Korolev, I.; Altınkaya, P.; Halli, P.; Hannula, P.-M.; Yliniemi, K.; Lundström, M. Electrochemical Recovery of Minor Concentrations of Gold from Cyanide-Free Cupric Chloride Leaching Solutions. *J. Cleaner Prod.* **2018**, *186*, 840−850.

(41) Halli, P.; Wilson, B. P.; Hailemariam, T.; Latostenmaa, P.; Yliniemi, K.; Lundström, M. Electrochemical Recovery of Tellurium from Metallurgical Industrial Waste. *J. Appl. Electrochem.* **2020**, *50* (1), 1−14.

(42) Halli, P.; Elomaa, H.; Wilson, B. P.; Yliniemi, K.; Lundström, M. Improved Metal Circular Economy-Selective Recovery of Minor Ag Concentrations from Zn Process Solutions. *ACS Sustainable Chem. Eng.* **2017**, *5* (11), 10996−11004.

(43) Korolev, I.; Spathariotis, S.; Yliniemi, K.; Wilson, B. P.; Abbott, A. P.; Lundström, M. Mechanism of Selective Gold Extraction from Multi-Metal Chloride Solutions by Electrodeposition-Redox Replacement. *Green Chem.* **2020**, *22* (11), 3615−3625.

(44) Halli, P.; Heikkinen, J. J.; Elomaa, H.; Wilson, B. P.; Jokinen, V.; Yliniemi, K.; Franssila, S.; Lundström, M. Platinum Recovery from Industrial Process Solutions by Electrodeposition−Redox Replacement. *ACS Sustainable Chem. Eng.* **2018**, *6* (11), 14631−14640.

(45) Wang, Z.; Halli, P.; Hannula, P.; Liu, F.; Wilson, B. P.; Yliniemi, K.; Lundström, M. Recovery of Silver from Dilute Effluents via Electrodeposition and Redox Replacement. *J. Electrochem. Soc.* **2019**, *166* (8), E266.

(46) Yliniemi, K.; Nguyen, N. T.; Mohajernia, S.; Liu, N.; Wilson, B. P.; Schmuki, P.; Lundström, M. A Direct Synthesis of Platinum/Nickel Co-Catalysts on Titanium Dioxide Nanotube Surface from Hydrometallurgical-Type Process Streams. *J. Cleaner Prod.* **2018**, *201*, 39−48.

(47) Hannula, P.-M.; Pletincx, S.; Janas, D.; Yliniemi, K.; Hubin, A.; Lundström, M. Controlling the Deposition of Silver and Bimetallic Silver/Copper Particles onto a Carbon Nanotube Film by Electrodeposition-Redox Replacement. *Surf. Coat. Technol.* **2019**, *374*, 305−316.

(48) Wang, W.; Li, R.; Yuan, T.; Zhu, X.; Li, H.; Lin, W.; Li, L. Effects of Ag+ in Diaphragm Electrolysis on Oxygen Evolution and Corrosion Behaviors of Pb and PbAg Anodes. *Hydrometallurgy* **2020**, *192*, 105254.

(49) Sorour, N.; Zhang, W.; Ghali, E.; Houlachi, G. A Review of Organic Additives in Zinc Electrodeposition Process (Performance and Evaluation). *Hydrometallurgy* **2017**, *171*, 320−332.

(50) Majuste, D.; Martins, E. L. C.; Souza, A. D.; Nicol, M. J.; Ciminelli, V. S. T. Role of Organic Reagents and Impurity in Zinc Electrowinning. *Hydrometallurgy* **2015**, *152*, 190−198.

(51) Sorour, N.; Zhang, W.; Gabra, G.; Ghali, E.; Houlachi, G. Electrochemical Studies of Ionic Liquid Additives during the Zinc Electrowinning Process. *Hydrometallurgy* **2015**, *157*, 261−269.

(52) Ornelas, J.; Marquez, M.; Genesca, J. Cementation Kinetics of an Industrial Solution of Ag(CN)2− with Granular Spherical Zinc in a Vibrating Reactor. *Hydrometallurgy* **1998**, *47* (2), 217−229.

(53) Mai, N. T.; Thuy, T. T.; Mott, D. M.; Maenosono, S. Chemical Synthesis of Blue-Emitting Metallic Zinc Nano-Hexagons. *CrystEngComm* **2013**, *15* (33), 6606−6610.

(54) Sato, R. Crystal Growth of Electrodeposited Zinc: An Electron Diffraction and Electron Microscopic Study. *J. Electrochem. Soc.* **1959**, *106* (3), 206.

(55) He, H.; Tong, H.; Song, X.; Song, X.; Liu, J. Highly Stable Zn Metal Anodes Enabled by Atomic Layer Deposited Al 2 O 3 Coating for Aqueous Zinc-Ion Batteries. *J. Mater. Chem. A* **2020**, *8* (16), 7836−7846.

(56) Zheng, J.; Zhao, Q.; Tang, T.; Yin, J.; Quilty, C. D.; Renderos, G. D.; Liu, X.; Deng, Y.; Wang, L.; Bock, D. C.; Jaye, C.; Zhang, D.; Takeuchi, E. S.; Takeuchi, K. J.; Marschilok, A. C.; Archer, L. A. Reversible Epitaxial Electrodeposition of Metals in Battery Anodes. *Science* **2019**, *366* (6465), 645−648.

(57) Thota, S.; Zhou, Y.; Chen, S.; Zou, S.; Zhao, J. Formation of Bimetallic Dumbbell Shaped Particles with a Hollow Junction during Galvanic Replacement Reaction. *Nanoscale* **2017**, *9* (18), 6128−6135.

(58) Giménez-Romero, D.; García-Jareño, J. J.; Vicente, F. EQCM and EIS Studies of Znaq2++2e−⇄Zn0 Electrochemical Reaction in Moderated Acid Medium. *J. Electroanal. Chem.* **2003**, *558*, 25−33.

(59) Giménez-Romero, D.; García-Jareño, J. J.; Vicente, F. Calculation of the Surface Concentration of Zn(I) from the Anodic Voltammetric Peak of Zinc Combined with the QCM Results. *Electrochem. Commun.* **2004**, *6* (9), 903−907.

(60) Achari, I.; Ambrozik, S.; Dimitrov, N. Electrochemical Atomic Layer Deposition of Pd Ultrathin Films by Surface Limited Redox

Replacement of Underpotentially Deposited H in a Single Cell. *J. Phys. Chem. C* **2017**, *121* (8), 4404−4411.